Oral Oncology (2006) 42, 914–928

available at www.sciencedirect.com

ScienceDirect

journal homepage: http://intl.elsevierhealth.com/journals/oron/

ORAL ONCOLOGY

Performance analysis of different wavelet feature vectors in quantification of oral precancerous condition

Anirban Mukherjee [a], Ranjan Rashmi Paul [b,c], Keya Chaudhuri [d], Jyotirmoy Chatterjee [e], Mousumi Pal [c], Provas Banerjee [c], Kanchan Mukherjee [f], Swapna Banerjee [g], Pranab K. Dutta [a,*]

[a] *Department of Electrical Engineering, Indian Institute of Technology, Kharagpur, 721 302 West Bengal, India*
[b] *Department of Oral and Maxillofacial Pathology, Guru Nanak Institute of Dental Science and Research, Panihati, Kolkata, India*
[c] *Institute of Interdisciplinary Scientific Research (IISR), 17B Ramchandra Maitra Lane, Kolkata, India*
[d] *Human Genetics and Genomics Group, Indian Institute of Chemical Biology, Kolkata, 700 032, India*
[e] *Department of Radiology (Diagnosis) Medical College Hospitals, Kolkata, 700 073, India*
[f] *Monovikas Kendra, 482, Madudah, Plot no.1—24, Sec-J Eastern Metropolitan, Bypass, Kolkata 700 107, India*
[g] *Department of Electronics and Electrical Communication Engineering, Indian Institute of Technology, Kharagpur, 721 302, India*

Received 21 November 2005; accepted 7 December 2005

KEYWORDS
Oral precancerous stage;
Oral submucous fibrosis;
Collagen;
Transmission electron microscopy;
Artificial neural network (ANN);
Wavelet

Summary This paper presents an automatic method for classification of progressive stages of oral precancerous conditions like oral submucous fibrosis (OSF). The classifier used is a three-layered feed-forward neural network and the feature vector, is formed by calculating the wavelet coefficients. Four wavelet decomposition functions, namely GABOR, HAAR, DB2 and DB4 have been used to extract the feature vector set and their performance has been compared. The samples used are transmission electron microscopic (TEM) images of collagen fibers from oral subepithelial region of normal and OSF patients. The trained network could classify normal fibers from less advanced and advanced stages of OSF successfully.

Introduction

Oral cancer is increasing at an alarming rate and it is the 11th most common cancer in the world. Out of a large number, two-third cases are recorded in developing

* Corresponding author. Tel.: +91 3222283054. fax: +91 3222282262.
E-mail address: pkd@ee.iitkgp.ernet.in (P.K. Dutta).

1368-8375/$ - see front matter © 2005 Elsevier Ltd. All rights reserved.
doi:10.1016/j.oraloncology.2005.12.008

countries.[1] A high incidence of oral cancer is mainly due to late diagnosis of potential precancerous lesions and conditions. There is consistent evidence that persons with early stage of oral cancer i.e., diagnosed at precancerous stage have a better prognosis than those diagnosed with more advanced state of the disease.[2] Oral submucous fibrosis (OSF) is such precancerous condition of oral cavity and oropharynx having insidious chronic progressive nature and a high degree of malignant potentiality.[3] A significant number (7.6%) of the pathosis may convert into squamous cell carcinoma (SCC).[3] This disease is now a public health concern in many parts of the world including United Kingdom,[4] South Africa [5] and many southeast Asian countries [6,7] though it is mainly prevalent in the Indian subcontinent in all age groups and across all socioeconomic strata.[6,7]

Interestingly, the aetiology of OSF is still ill understood but varied addictive oral habits have shown strong correlation with the etiology of this disease. Arecoline, an active alkaloid found in betel nuts have been reported to stimulate fibroblasts with 150% increase in collagen production.[8] Besides oral habits, other factors like ingestion of chilies, deficiencies of nutritional elements including trace metal and vitamin, hypersensitivity to various dietary constituents and genetic as well as immunological predisposition are suggested to be involved in the progression of this pathosis.[9,10]

Presently, in the diagnosis and assessment of this disease state clinicians normally rely on the empirical light microscopic histopathological evaluation of OSF biopsies integrated with clinical evaluation. Histopathologically OSF is characterized by less vacularized collagenous connective tissue with concomitant presence of atrophic overlying epithelium, which may be associated with variable degrees of dysplastic changes.[11] Atrophy of the muscle fibers and varied degree of chronic inflammatory infiltrate are also recorded in the diseased tissue. Clinically, varied degrees of trismus (inability to open the mouth) in these patients are also evident which has a direct correlation with the oral location of the OSF lesion and degree of fibrosis due to excessive formation of subepithelial collagen fibers. Thus, in this disease process, though both epithelium and connective tissue are involved but malignancy becomes evident in the epithelium only. Here lies the question: which part of the oral mucosa is more contributory in the development of such precancer condition. Physiologically, avascular oral epithelium is dependent on the underlying vascularized connective tissue for nutrition. In this disease process the excessive formation of collagen in the subepithelial mucosa obliterates the blood vessels, which possibly leads to the nutritional impairment at the overlying epithelium. This condition of the epithelium along with concurrent carcinogenic insult on the oral epithelium by addictive oral habits possibly favors the progression of such disease process.[12]

Interestingly, very few studies have addressed the collagen changes and fibrosis in a definite quantitative manner. Ultrastructural studies on subepithelial collagen fibers in OSF and normal mucosa have noted variation in their width and periodicity qualitatively.[13] Keeping these facts in mind, the transmission electron micrographs of subepithelial fibrillar collagen population of early and advanced stages of OSF has been analyzed to compare the same with that of normal oral mucosa by computer aided diagnostic (CAD) approach coupled with wavelet-ANN.[14] The CAD refers to a diagnostic process in which a radiologist uses a computer analysis as a diagnostic aid to achieve more accurate interpretation of the disease state. In this work, the precancer diagnostic importance of CAD system coupled with wavelet-ANN has been studied by analyzing the OSF and normal oral mucosal collagen. The wavelet transform technique is ideal for teasing out information from signals that are aperiodic, noisy, intermittent or transient. ANN is an important statistical tool [15] to improve the characterization of pathological images especially of precancer and cancers. Few reports are available regarding successful applications of machine learning in precancerous diagnosis.[16–20] Thus this study would strengthen the foundation of ANN in CAD applications. In countries like India CAD-based software has special importance because it provides a low-cost solution for first hand measure of the patient's state of disease.

A number of literatures are available in wavelet based feature extraction,[21] which is found to be useful in cancer and precancer research also. Wavelet-based texture parameters or other kind of texture features may be possible to be corresponded to normal and advanced stages of precancer. However, less-advanced stages have lot of overlapping features with both normal and advanced stages. Even some of the advanced stages have overlapping features with normal ones. In such cases, ANN-based classifiers perform in a better way.

This paper has been organized in the following way: The next section i.e., second section discusses about the selection and clinical classification of test cases and electron microscopic methodology of preparing this test data. Third section has presented an exhaustive overview of wavelet-ANN based analysis of the test images. More specifically, first part has focused on Gabor filter-based texture classification methodology. Second part has described wavelet-based technique to capture the texture information of the test images. Fourth describes the background of ANN and its use as the pattern classifier. ANN tries to capture the signature (pattern) as a reflection of the stage of OSF, namely, normal, less-advanced or advanced. Fifth section illustrates the performance of various wavelets as a performance measure for the detection of the disease. Finally, the last section concludes this paper.

Selection of patients, clinical classification of OSF stages and transmission electron microscopic (TEM) study

Selection of patients

Clinically diagnosed OSF patients were subjected to incisional biopsy with their prior consent at the Department of Oral and Maxillofacial Pathology, R. Ahmed Dental College & Hospital, Kolkata for histopathological evaluation. A portion from each biopsy tissue of oral mucosa of the clinically and histologically confirmed cases of early ($n = 55$) and advanced ($n = 60$) stages of OSF were taken for the analysis of fibrillar collagen ultrastructure by transmission electron microscope. The normal healthy volunteers ($n = 30$) of similar age and food habits but without oral habit were also included in the study.

Clinical classification of OSF stages

The classification/grading of the disease OSF has been done according to the degree of trismus, which has direct correlation with degree of fibrosis, progression of the disease and location of the OSF lesion in oral mucosa. Trismus or reduction in the overall mouth opening is one of the most prudent manifestations of OSF [11,13] and it has been a cardinal clinical feature to grade the patients into different groups. The gradation of trismus and in turn gradation of the disease process was done by measuring the distance between the incisal edges of the upper and lower central incisal teeth i.e., the interincisal distance (IID), by vernier calipers as follows: mild or moderate grade ($1.5\ \text{cm} \leqslant \text{IID} < 3.5\ \text{cm}$) and severe grade ($\text{IID} < 1.5\ \text{cm}$) considering $\text{IID} \geqslant 3.5$ as normal.

Transmission electron microscopic (TEM) study

Biopsy samples of 1 mm × 2 mm were fixed in primary fixative (2.5% glutaraldehyde in 0.12 M phosphate buffer) for 48 h at 4 °C. The tissues were then washed in 0.12 M phosphate buffer and post-fixed in 2% osmium tetroxide for 2 h at room temperature with constant shaking. Following post fixation, tissues were dehydrated in graded alcohol and processed for spur embedding. Ultrathin sections were made by Nova Ultratome (LKB), collected on copper grids and stained with uranyl acetate and lead citrate.[13,22] Sections were observed under transmission electron microscope (JEOL 100CX TEM) operated at 60 KV.

Wavelet-ANN-based analysis of TEM images of collagen

In this study a wavelet-ANN-based novel scheme has been proposed for the detection and grading of OSF stages (advanced and less advanced) by analyzing TEM images of subepithelial collagen fibers (shown in Fig. 1a—f), taken randomly from a population ($n = 145$) consisting of 55 less advanced and 60 advanced OSF patients and 30 normal healthy volunteers.

Through random sampling, a set of 145 image samples (dimension 64 × 64 pixels, as shown in Fig. 2a—d) of subepithelial collagen image data has been taken to make a large training set. Accordingly, this technique grabbed the said 145 image samples from 5, 5, 7 representative subepithelial TEM collagen images of normal volunteers, less advanced and advanced stages of OSF patients respectively. This 64 × 64 image has been decomposed into various bands. The feature vector has been judiciously chosen from the subband images. It has been assumed that the feature vector has captured the signature of stage of the disease. These feature vectors are used to train the ANN. During the test, the images are decomposed into 64 × 64 non-overlapping blocks. The feature vectors have been extracted for each block and fed to the ANN. The output may be of three different types: normal, less advanced and advanced stage of OSF. Based on the number of blocks in each of these three classes, a decision has been taken for the image under test.

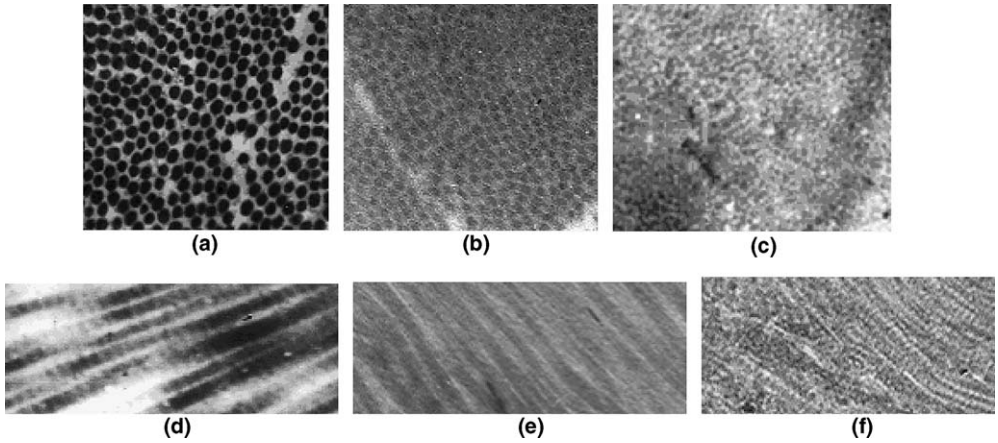

Figure 1 TEM images of collagen normal (a,d) less advanced (b,e) advanced (c,f) stage of OSF, (a—c) represent transverse sections and (d—f) represent longitudinal sections of collagen fibers, respectively.

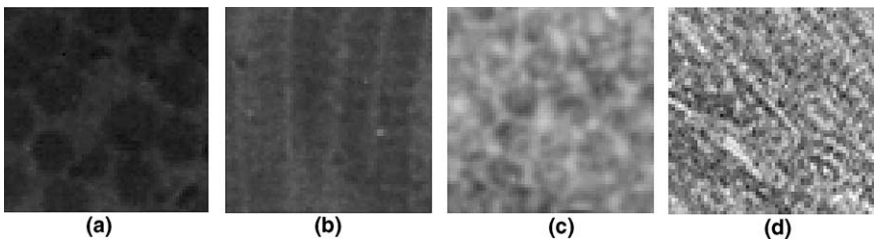

Figure 2 Training 64 × 64 sample TEM image of oral subepithelial collagen (TS): (a) normal transverse; (b) normal longitudinal; (c) advanced stage of OSF transverse; (d) advanced stage of OSF longitudinal.

In the next section, Gabor filter has been introduced as a texture characterizing filter along with three wavelet filters. The background of these filters and the choice of feature vector have been described in detail.

Gabor filter-based feature vector extraction

The filter structure for analyzing textured image has been assumed as $m(x,y) = \text{-}i(x,y)^{*} f(x,y)\text{-}$, where $i(x,y)$ and $f(x,y)$ are the image and Gabor elementary function (GEF) respectively. The GEF has the following interesting properties:

1. The GEF's are the only functions that achieve minimum space bandwidth product as specified by uncertainty principle [23] $\Delta U = \Omega X < \frac{1}{2}$, where Ω and X are the spreads in frequency and space domains respectively. This means that GEF can be designed to be optimally selective in spatial frequency while oering good spatial localization.
2. GEF's are the set of band pass filters. They can be judiciously tuned to extract a specific band of frequency components.
3. The shape of GEF's resemble the receptive field profiles of simple cells in a visual pathway.

GEF's were first defined by Gabor [24] and Daugman [25] extended it to double dimensions. A few researchers refer GEF as Gabor wavelets.[26,27] The Gabor function do not exactly satisfy the requirements that the wavelet be admissible and progressive.[28] However, in the context of representing a class of self-similar functions, this term is used. In the spatial domain, the Gabor function is a complex exponential modulated by a Gaussian function. The Gabor function forms a complete but a non-orthogonal basis set and its impulse response in the two-dimensional (2-D) plane has the following general form:[28]

$$f(x,y) = \frac{1}{2\pi\sigma_x\sigma_y}\exp\left[-\frac{1}{2}\left(\frac{x^2}{\sigma_x^2}+\frac{y^2}{\sigma_y^2}\right)\right]\exp(2\pi j u_0 x) \tag{1}$$

where u_0 denotes the radial frequency of the Gabor function. The constants σ_x and σ_y defines the spread of Gabor envelop along x and y axes. In the frequency domain, the Gabor function acts as a band pass filter and the Fourier transform of $f(x,y)$ is given by

$$F(u,v) = \exp\left[-\frac{1}{2}\left\{\frac{(u-u_0)^2}{\sigma_u^2}+\frac{v^2}{\sigma_v^2}\right\}\right] \tag{2}$$

where $\sigma_u = \frac{1}{2\pi\sigma_x}$ and $\sigma_v = \frac{1}{2\pi\sigma_y}$.

A class of self-similar functions, referred as Gabor wavelets, has been considered in this work for signature classification of stage of the disease. Using (1) as the mother Gabor wavelet, the self-similar filter bank can be obtained by appropriate scaling and rotation of the generating function

$$f_{pq}(x,y) = \alpha^{-p} f(x',y') \tag{3}$$

where $x' = \alpha^{-p}(x\cos\theta_q + y\sin\theta_q)$ and $y' = \alpha^{-p}(-x\sin\theta_q + y\cos\theta_q), \alpha > 1, p = 0,1,2,\ldots,S-1$ and $q = 0,1,2,\ldots,L-1$. The integer subscripts p and q represent the index for scale (dilation) and orientation (rotation), respectively. S is the total number of scales and L is the total number of orientations in the self-similar Gabor filter bank. For each orientation q, the angle θ_q is given by $\frac{\pi q}{L}$, $q = 0,1,2,\ldots,L-1$. The scale factor α^{-p} ensures that the energy $E_{pq} = \int_{-\infty}^{\infty}\int_{-\infty}^{\infty}|f_{pq}(x,y)|^2\,dx\,dy$ is independent of p.[28]

Thus, all the filters in the Gabor filter bank have the same energy, irrespective of their scale and orientation. In,[28] a bank of self-similar Gabor filters has been formed by rotation (varying) and dilation (varying) of the basic Gabor filter (1). They are used to compute the texture signature of the OSF images. Each of the complex Gabor filters has the real and imaginary parts that are conveniently implemented as the spatial mask of $M \times M$ sizes. In order to have a symmetric region of support, M is preferred to be an odd number. For a given input image $I(x,y)$, the magnitude of filtered image $M_{pq}(x,y)$ is obtained by using Gabor filter $f_{pq}(x,y)$ as follows:

$$M_{pq}(x,y) = \left\{\text{real}(f_{pq}(x,y) * I_{pq}(x,y))^2 + \text{imag}(f_{pq}(x,y) * I_{pq}(x,y))^2\right\}^{0.5} \tag{4}$$

The non-orthogonality of Gabor wavelets implies that there is redundant information in the filtered images $M_{pq}(x,y)$ of dimension 64×64. The following strategy is adopted to reduce this redundancy. Let U_h and U_l denote the upper and lower center frequencies of interest. In,[28] the factor α and frequency spreads in x and y direction have been computed such that half peak magnitude cross-section of the filter responses touch each other.

In the present work, the number of scales S and orientations L are assumed to be 5 and 4, respectively with mask size 21×21. The feature vector has been computed by the mean of the filtered image $\mu_{pq} = \sum_x\sum_y\|M_{pq}(x,y)\|^2$. The feature vector has been defined as FV = $[\mu_{00}\ \mu_{01}\ \ldots\ \mu_{54}]^T$. These feature vectors have been fed to train the ANN.

Wavelet and subband decomposition and feature vector extraction [29–31]

Sub-band decomposition has been carried out here for the case of 2-D signals. As mentioned in the previous section,

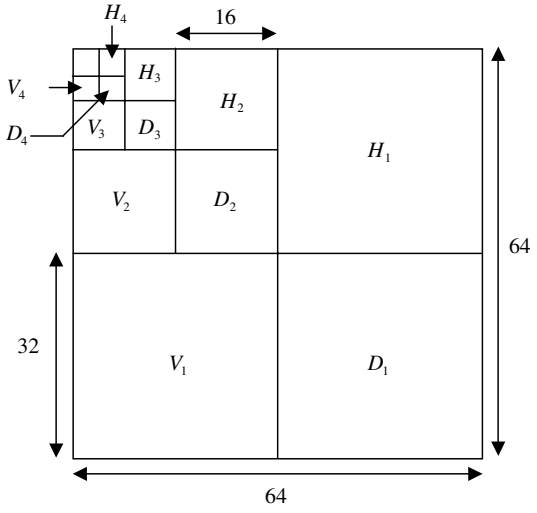

Figure 3 Wavelet decomposition of 64×64 training image sample.

a number of 64×64 image templates have been taken in order to extract the feature vector for training the ANN. Figure 2 shows four such training samples, two for normal cell and other for advanced stage of disease. These sample images have been decomposed by HAAR, DB2 and DB4 wavelet into four levels. In each level, there are three sets of detail coefficients: horizontal (H_i), vertical (V_i) and diagonal (D_i), $i = 1, 2, 3, 4$ as shown in Figure 3. The dimension of H_i is $64 * 2^{-i} \times 64 * 2^{-i}$. It is same for V_i and D_i also. These H_i, V_i and D_i have been extracted by using 'detcoef2' function of MATLAB 7.[28] The four approximation coefficients, A_i, have been extracted from the four levels by using 'appcoef2'. The Frobenious norm [32] has been computed for H_i, V_i, D_i and A_i and denoted as $\|\bullet\|_F$. The element of the feature vector (FV) is the Frobenious norm of H_i, V_i, D_i and A_i. $FV = [\|H_i\|_F \|V_i\|_F \|D_i\|_F k \|A_i\|_F]^T$ $i = 1, 2, 3, 4$ where k is set as 0.001. These feature vectors have been fed to train the ANN.

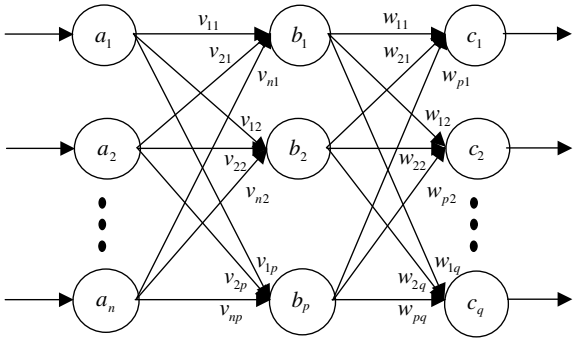

Figure 4 Weight vectors in the MLP feed-forward network.

Table 1 Correlation between feature vectors of normal (N), less-advanced (L) and advanced (A) stage of disease for four different wavelet functions

	HAAR	DB2	DB4
(N—L)	0.814	0.831	0.905
(N—A)	0.609	0.761	0.721
(L—A)	0.905	0.608	0.701

Multi-layered perceptron (MLP) feed-forward neural network

It has been proved that a three-layered network can represent a non-linear function of any order.[33] The number of layers and number of nodes in the hidden layer are guided by many practical aspects, e.g., redundancy, number of input training set, spurious oscillations etc. However, the most critical part of an ANN-based model is to train the network. The network has been shown in Figure 4. In this figure v_{ij} and w_{pq} denote the weights for the successive layers. The basic purpose of training a network is to optimize v_{ij} and w_{pq} corresponding to a particular set of input-output training pattern.

The responses at the hidden nodes b_j, $j = 1, 2, \ldots, p$ are calculated by evaluating the contributions from all the input nodes through a non-linear mapping function.

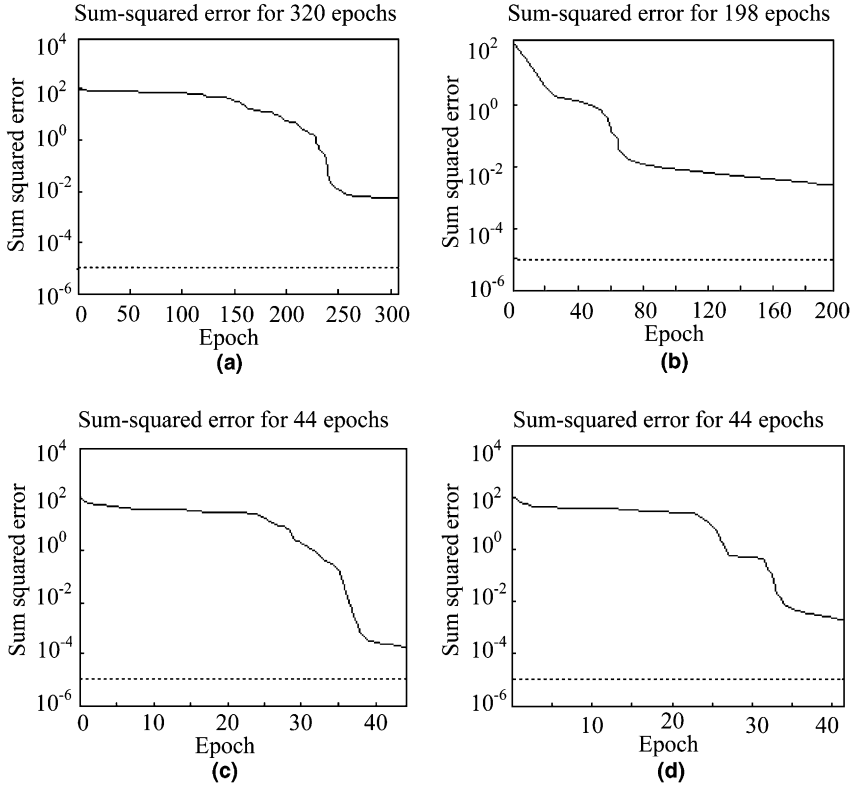

Figure 5 Convergence of ANN training with (a) Gabor, (b) HAAR, (c) dB2, (d) dB4 wavelet basis.

$$b_j = f\left[\sum_{i=1}^{n} a_i v_{ij} + \theta_j\right] \quad (5)$$

where the function $f(\bullet)$ chosen is the 'tansig' function of MATLAB 7. The tansig function is given by $\frac{2}{1+\exp(-2n)} - 1$. θ_j is the bias at the jth hidden layer node and a_i is the input vector. Similarly, c_k, $k = 1, 2, \ldots, q$ is calculated using

$$c_k = f\left[\sum_{j=1}^{n} b_j w_{jk} + \tau_k\right] \quad (6)$$

where τ_k is the bias at the kth output layer node.

The function 'trainlm' in the neural network toolbox [34] in MATLAB 5.1 has been used for training the network. It uses a mixture of Gauss–Newton method and gradient descent technique for optimization of the weights, w_{jk} and v_{ij}. The Levenberg–Marquardt weight update rule is

$$\Delta w = (J^T J + \mu I)^{-1} J^T e \quad (7)$$

where J is the Jacobian matrix of derivatives of each error to each weight, μ is a scalar, I is the identity matrix and e is an error vector. Training continues until the error goal is met and the minimum error gradient occurs.

Justification of using ANN as a pattern classifier

ANN has been used as a pattern classifier in this present work. In,[35] a number of methods for training the classifiers

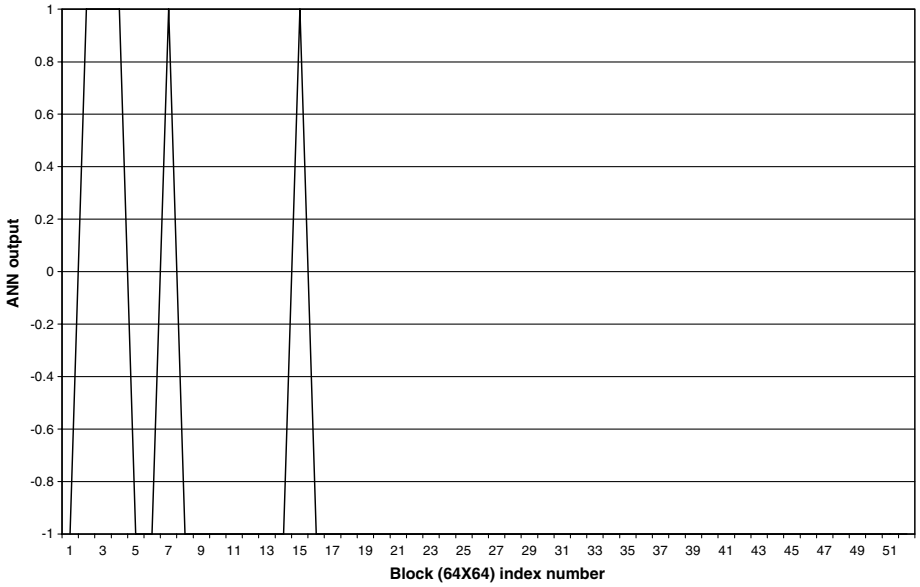

Figure 6 ANN output for an image of normal cells with HAAR wavelet.

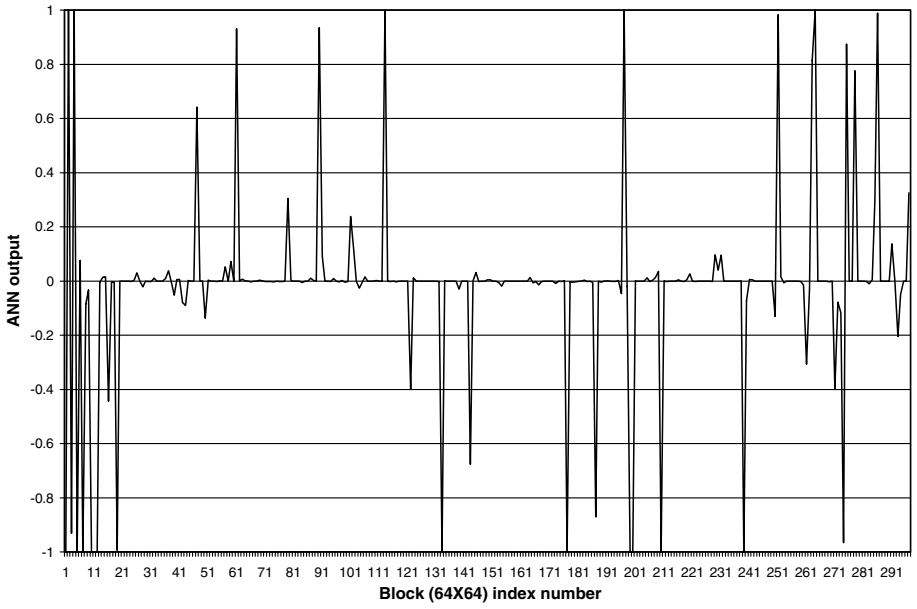

Figure 7 ANN output for an image of less-advanced stage of OSF with HAAR wavelet.

have been described. The pattern classification has been formulated as to estimate the minimum misclassification error. The least-mean-square (LMS) algorithm provides a powerful gradient decent method for reducing the error, even when pattern are not linearly separable in feature space. The class of solutions, comprising hyperplane decision boundaries, has many problems for which linear discriminants are insufficient for minimum error. With a clever choice of non-linear discriminant functions, the arbitrary decision regions can be achieved leading to minimum classification error. The central difficulty is choosing the appropriate non-linear functions. ANN is a way to learn the non-linearity. The parameters governing the non-linear mapping are learned at the same time as those governing the linear discriminant. Table 1 shows the correlation of sample training feature vector of three different classes namely normal, less-advanced and advanced. Four wavelet functions have been considered. But, the feature vectors formed by the other wavelet functions have high degree of similarity in nature. In case of HAAR wavelet-based analysis, a sample less-advanced feature vector is similar with the advanced one with a degree of similarity 0.905. As the feature vectors are highly overlapping in feature space, ANN may be the right technique for pattern classification in this work.

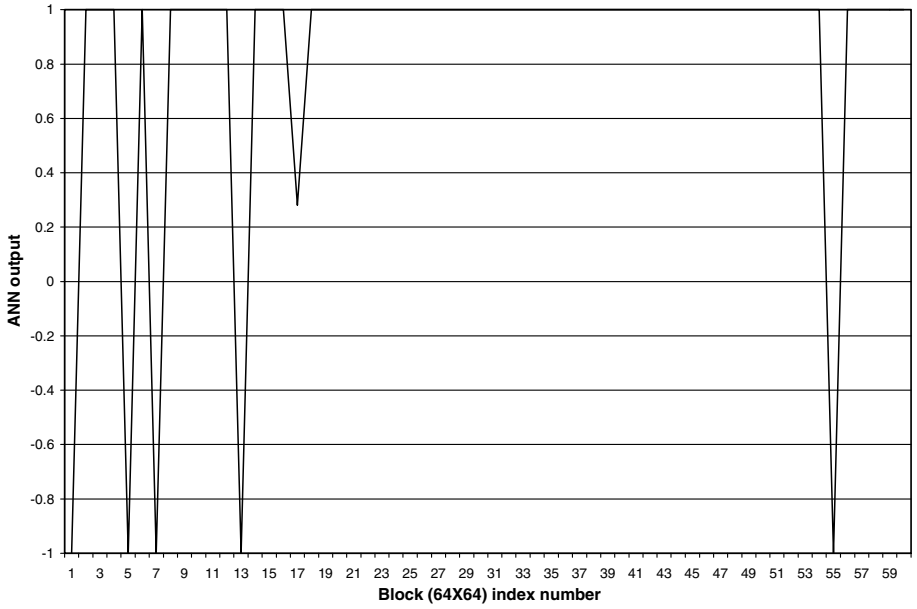

Figure 8 ANN output for an image of advanced stage of OSF with HAAR wavelet.

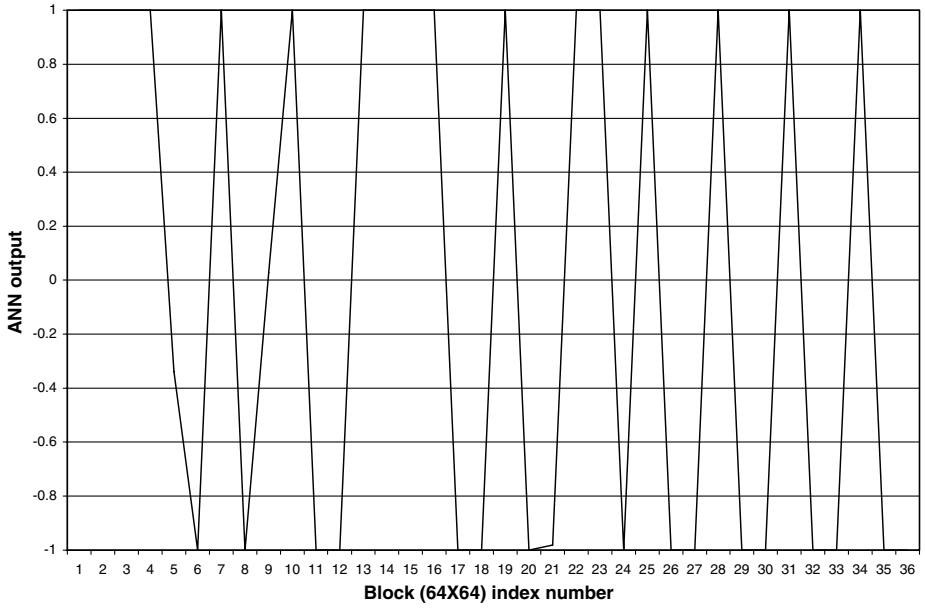

Figure 9 ANN output for an image of normal cells with GABOR wavelet.

Training by ANN

In the present work, a three-layered ANN has been used. A single hidden layer with 6 and 4 neurons is found to be sufficient for training with Gabor and HAAR wavelet respectively as shown in Figure 5. Similarly, the convergence pattern has also been shown for DB2 and DB4 wavelets in the same figure. Convergence has been achieved within 320 epochs in case of Gabor wavelet. In case of HAAR wavelet, ANN converges within 200 epochs. The maximum number of epochs has been fixed at 400. The sum squared error goal has been kept at 10^{-5}. The learning rate and minimum feasible gradient are chosen as 0.01 and 0.05 respectively for both the cases. The detailed discussions of these parameters are available in.[33]

Results and discussion

After successful training, a number of images from different patients have been randomly taken for testing. The feature vector has been extracted from each of the contiguous 64×64 pixel blocks by wavelet (Gabor, HAAR, DB2, DB4) decomposition. These test feature vectors have been fed to ANN. The ANN outputs for three different test images are represented in Figures 6—8 in case of HAAR wavelet. The target output has three different states, denoted as

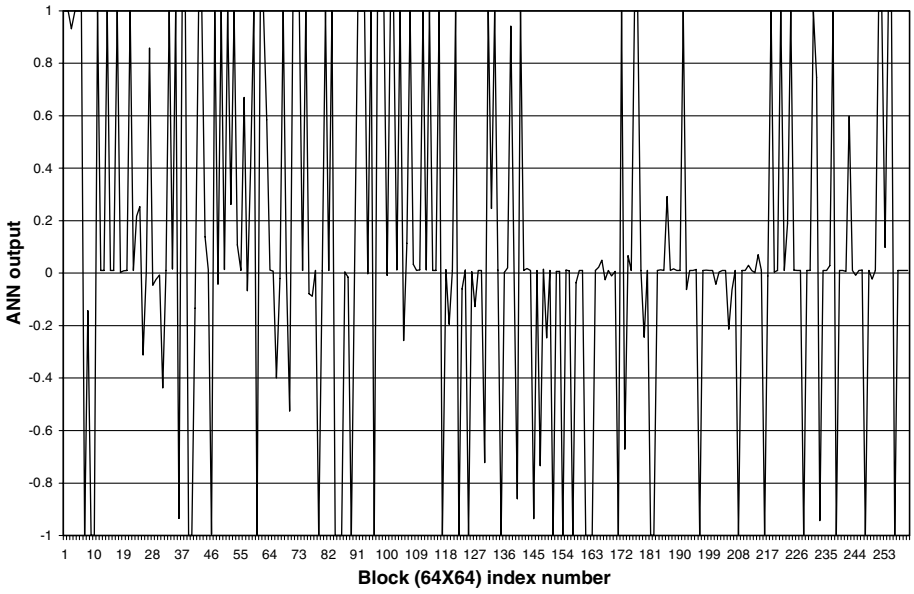

Figure 10 ANN output for an image of less-advanced stage of OSF with GABOR wavelet.

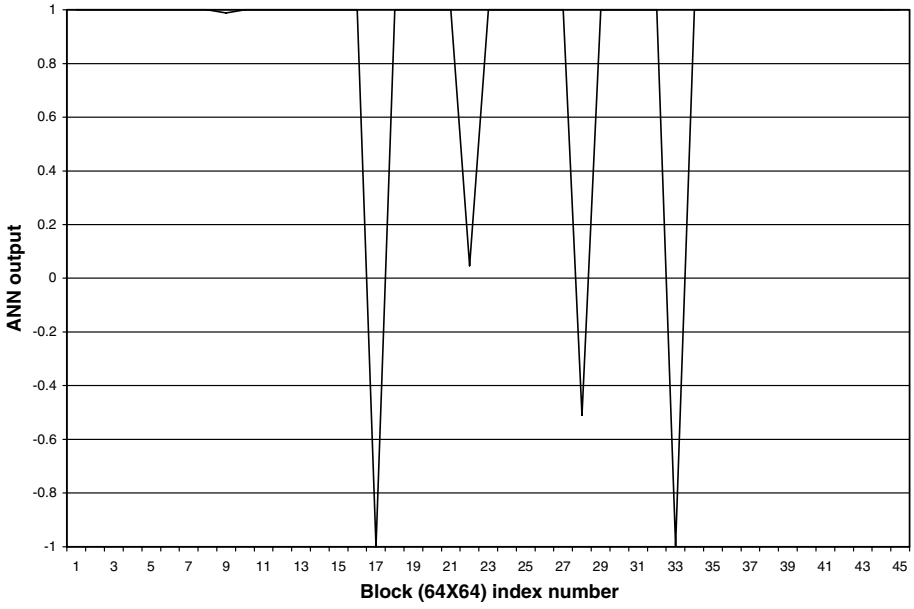

Figure 11 ANN output for an image of advanced stage of OSF with GABOR wavelet.

−1, 0 and +1. The states −1, 0 and +1 represent normal, less-advanced and advanced stages of OSF respectively. In case of untrained test samples, it may happen that the output of ANN for a particular 64×64 pixel block is not mapped exactly to three states i.e., say for a 64×64 pixel block sample of advanced state of disease, it may produce the output of +0.9 instead of +1.0. Naturally, a band around these three states needs to be defined. These bands correspond to Normal as well as less-advanced and advanced diseased states. The bands have been chosen as follows: If the output of 64×64 pixel block is less than −0.5, the block has been considered as ''normal'' block. A particular block has been treated as a ''less-advanced'' block, if the corresponding output is within the limit of −0.5 to +0.5. Similarly, if the output of a 64×64 pixel block is greater than +0.5, it has been treated as ''Advanced'' block.

In Figure 6, a normal image has been tested and the target output of each such 64×64 pixel block is set as −1 with HAAR basis function. There are 60 blocks of dimension 64×64 pixels. Out of these, only nine blocks are miss-classified as the target output of nine blocks is out of tolerance band. Similarly, in Figure 6, the test image is of less-advanced state of disease and the target output is set as 0. Out of total number of 297 blocks, 26 blocks are wrongly classified in Figure 7. In Figure 8, the test image is of advanced stage of the disease and the

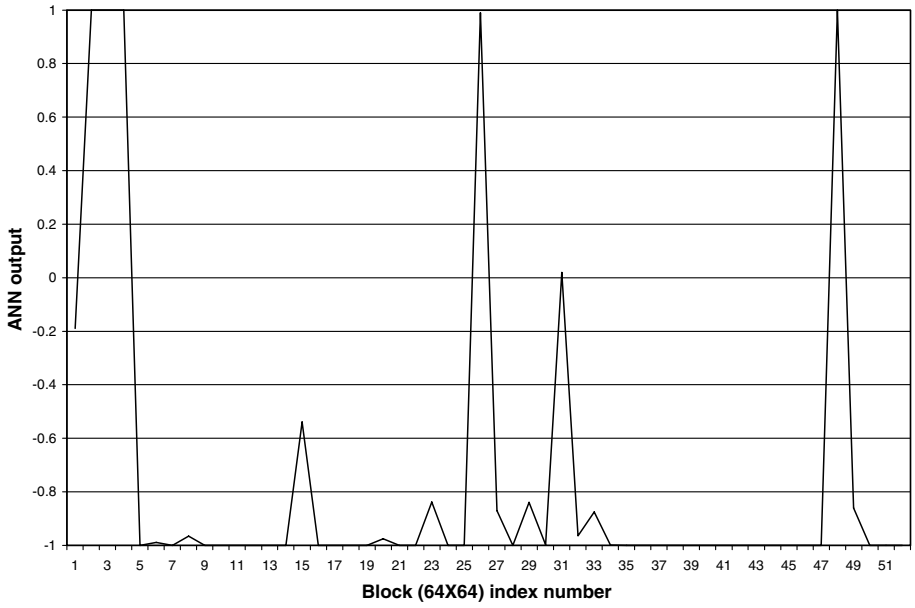

Figure 12 ANN output for an image of normal cells with DB2 wavelet.

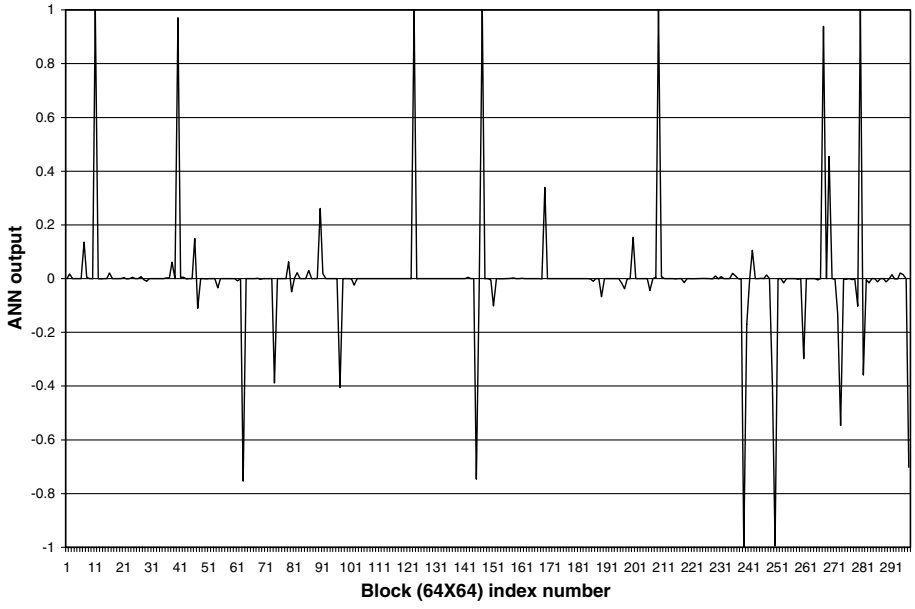

Figure 13 ANN output for an image of less-advanced stage of OSF with DB2 wavelet.

target output is set as +1. Out of 60 blocks only 6 blocks do not exhibit the correct signature. Figures 9–11 show the ANN output of Gabor wavelets for the normal, less-advanced and advanced stage of disease respectively. The corresponding outputs for DB2 and DB4 have been shown in Figures 12–17.

In order to give a measure of the efficiency of the proposed ANN-based scheme, a metric namely, Properly Classified Block Index (PCBI) has been computed for all the test images. PCBI has been defined as follows: PCBI $= \frac{N^P}{N^T} \times 100\%$, where N^P and N^T are the total number of properly classified 64×64 pixel blocks and total number of 64×64 pixel blocks in the test image. After classifying the blocks onto three states $-1, 0$ and $+1$, the number of blocks in each state has been computed. The number of properly classified blocks, N^P, has been taken as the maximum of these three counts. Based on the magnitude of PCBI, the final diagnosis has been performed about the nature of test images. A binary decision has been taken based on PCBI. If PCBI is greater than 50% (Fig. 18), it has been inferred that the correct diagnosis has been taken by the developed Wavelet-ANN-based system.

In Tables 2–5, 17 test images have been considered to check the diagnostic ability of the proposed wavelet ANN-based system. The first 5 images (index 1–5) are of normal state of OSF. It has been marked as ''N''. The less-advanced

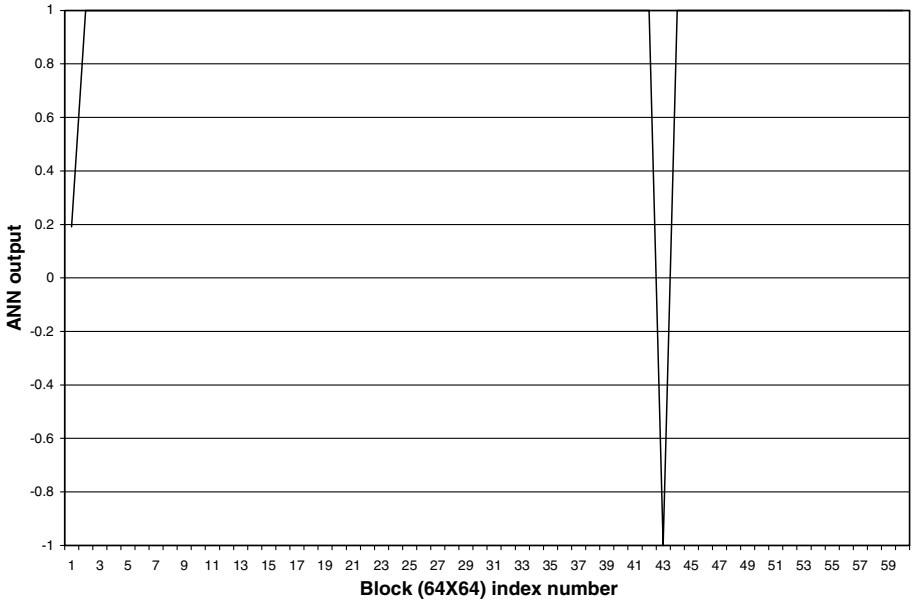

Figure 14 ANN output for an image of advanced stage of OSF with DB2 wavelet.

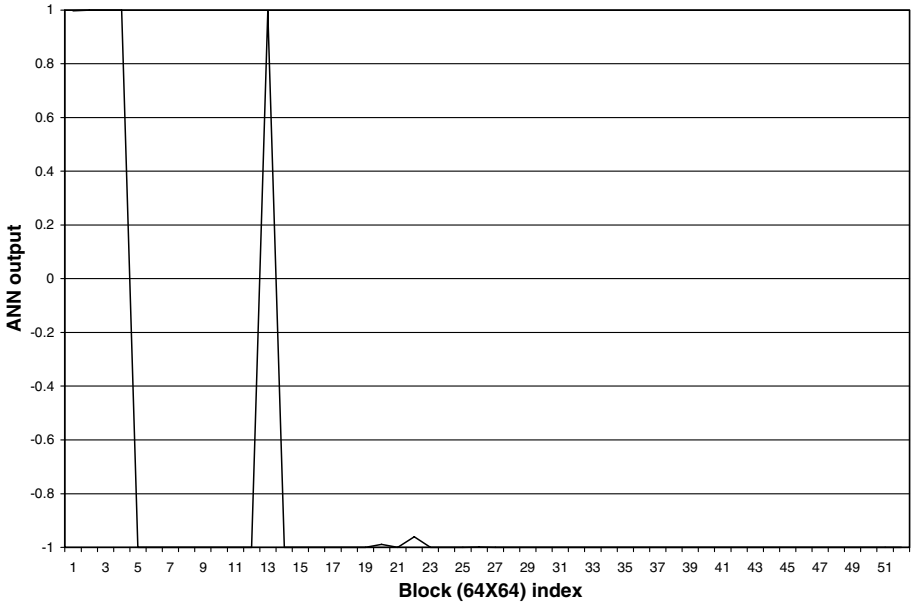

Figure 15 ANN output for an image of normal cells with DB4 wavelet.

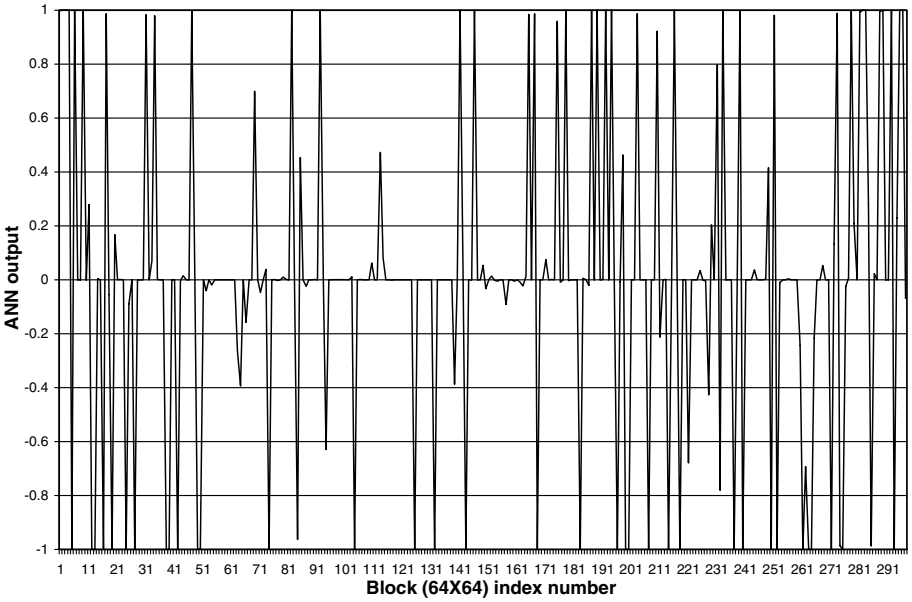

Figure 16 ANN output for an image of less-advanced stage of OSF with DB4 wavelet.

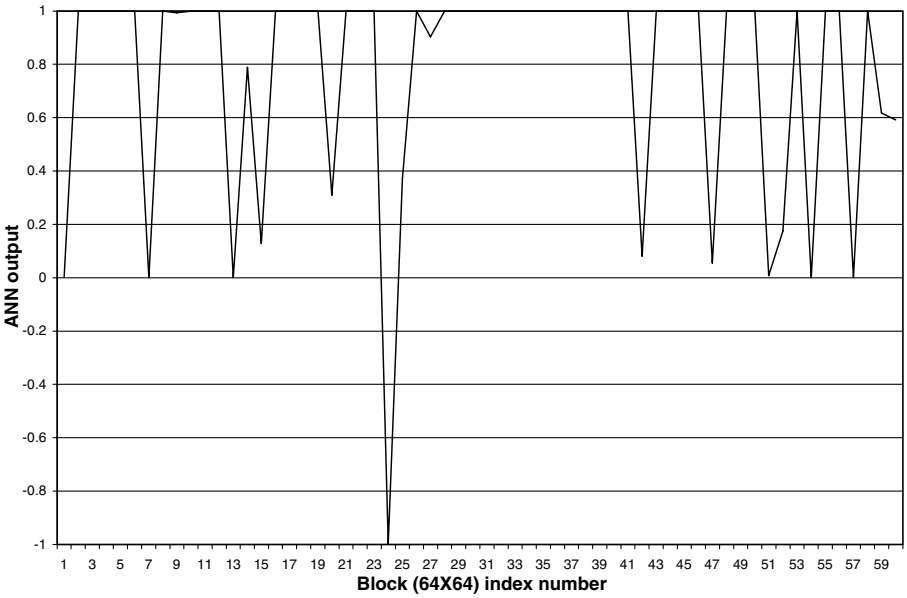

Figure 17 ANN output for an image of advanced stage of OSF with DB4 wavelet.

and advanced state of diseased images have been marked as ''L'' and ''A'' respectively.

It has been observed that the performance of Gabor filter is critical in characterizing both the images of normal and less-advanced stage. But it is performing well in case of advanced state of OSF. On the contrary, it has been found that

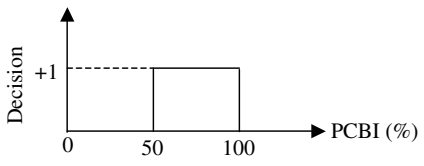

Figure 18 Binary decision for OSF stage detection.

all the test images are diagnosed properly by the proposed system with HAAR and DB2 basis functions. The DB4-based methodology has failed to properly classify one test image of less-advanced stage (Image index 6 in Table 5).

Figures 19—21 show the value of PCBI for all the 17 representative test images (5 normal, 5 less-advanced and 7 advanced stage of OSF) with different wavelet functions. It has been found from Figures 19 and 20 that HAAR is the most competent technique to successfully classify the normal condition and less advanced stage of disease whereas in case of advanced state, all the techniques are relatively performing well (Fig. 21).

PCBI gives the confidence measure of this automatic diagnostic methodology. It is important to note that this

Table 2 Results for GABOR wavelet, hidden layer node = 6 PCBI (%) = max (normal, less-advanced, advanced blocks) in %

Image index	Normal 64 × 64 blocks (%)	Less-advanced 64 × 64 blocks (%)	Advanced 64 × 64 blocks (%)
1 (N)	33.33	46.67	20.00
2 (N)	47.22	5.55	47.22
3 (N)	37.14	22.86	40.00
4 (N)	54.76	10.32	34.92
5 (N)	78.70	10.93	10.37
6 (L)	34.38	50.00	15.62
7 (L)	15.77	58.46	25.77
8 (L)	10.29	61.71	28.00
9 (L)	14.80	43.09	44.11
10 (L)	18.42	30.70	50.87
11 (A)	0.88	9.65	89.47
12 (A)	13.89	4.17	81.94
13 (A)	3.24	10.19	86.57
14 (A)	2.38	15.48	82.14
15 (A)	6.67	2.22	91.11
16 (A)	10.39	1.29	88.31
17 (A)	10.93	0.88	88.18

Table 3 Results for HAAR wavelet, hidden layer node = 4 PCBI (%) = max (normal, less-advanced, advanced blocks) in %

Image index	Normal 64 × 64 blocks (%)	Less-advanced 64 × 64 blocks (%)	Advanced 64 × 64 blocks (%)
1 (N)	80.00	16.67	3.33
2 (N)	86.54	3.85	9.62
3 (N)	56.82	4.55	38.64
4 (N)	87.33	4.67	8.00
5 (N)	75.34	2.72	21.94
6 (L)	22.22	73.33	4.44
7 (L)	4.38	91.25	4.37
8 (L)	0.96	95.19	3.85
9 (L)	2.56	95.73	1.71
10 (L)	6.41	91.03	2.56
11 (A)	22.14	0.71	77.14
12 (A)	14.29	14.29	71.43
13 (A)	6.47	6.07	87.45
14 (A)	5.77	4.81	89.42
15 (A)	1.67	11.67	86.67
16 (A)	4.16	4.16	91.67
17 (A)	16.5	3.89	79.50

Table 4 Results for DB2 wavelet, hidden layer node = 5 PCBI (%) = max (normal, less-advanced, advanced blocks) in %

Image index	Normal 64 × 64 blocks (%)	Less-advanced 64 × 64 blocks (%)	Advanced 64 × 64 blocks (%)
1 (N)	65.00	13.33	21.67
2 (N)	86.54	3.85	9.61
3 (N)	60.23	22.73	17.05
4 (N)	85.33	4.00	10.67
5 (N)	57.99	12.93	29.08
6 (L)	28.89	46.67	24.45
7 (L)	2.02	95.62	2.36
8 (L)	24.52	55.77	19.71
9 (L)	13.67	59.26	27.06
10 (L)	12.17	64.10	23.72
11 (A)	13.57	8.57	77.86
12 (A)	4.39	0.00	95.61
13 (A)	15.39	3.64	80.98
14 (A)	16.35	6.73	76.92
15 (A)	1.67	1.67	96.67
16 (A)	12.5	1.04	86.46
17 (A)	17.21	1.13	81.65

Table 5 Results for DB4 wavelet, hidden layer node = 5 PCBI (%) = max (normal, less-advanced, advanced blocks) in %

Image index	Normal 64 × 64 blocks (%)	Less-advanced 64 × 64 blocks (%)	Advanced 64 × 64 blocks (%)
1 (N)	63.33	3.33	33.33
2 (N)	90.39	0.0	9.62
3 (N)	60.23	6.82	32.95
4 (N)	81.33	2.67	16.0
5 (N)	61.91	4.59	33.50
6 (L)	28.89	31.11	40.0
7 (L)	14.14	72.39	13.47
8 (L)	7.69	55.77	36.54
9 (L)	2.85	81.48	15.67
10 (L)	2.56	91.00	6.44
11 (A)	16.43	2.14	81.43
12 (A)	12.03	7.69	80.22
13 (A)	10.53	7.29	82.19
14 (A)	14.42	8.65	76.92
15 (A)	1.67	20.0	78.33
16 (A)	15.61	27.08	57.29
17 (A)	21.59	4.54	73.86

result correspond to a training set of overlapping features, i.e., the blocks marked as advanced may contain a few normal or less-advanced cell also. This is similar to actual diagnosis scenario, where proper classification of all the cells in a sample is impossible to perform. The target stages of the training samples have been determined by looking at the overall features and corresponding to pathological stages inferred from other modalities also.

In empirical histopathological studies every clinical histopathologist tries to interpret the tissue changes and conditions more accurately but the accuracy differs from person to person depending on their level of perception and clinical acumen. Likewise in this study we have used four methods namely, Gabor, HAAR, DB2 and DB4, to classify the disease situation in a more quantitative manner with higher accuracy. The results show that HAAR is more effective in

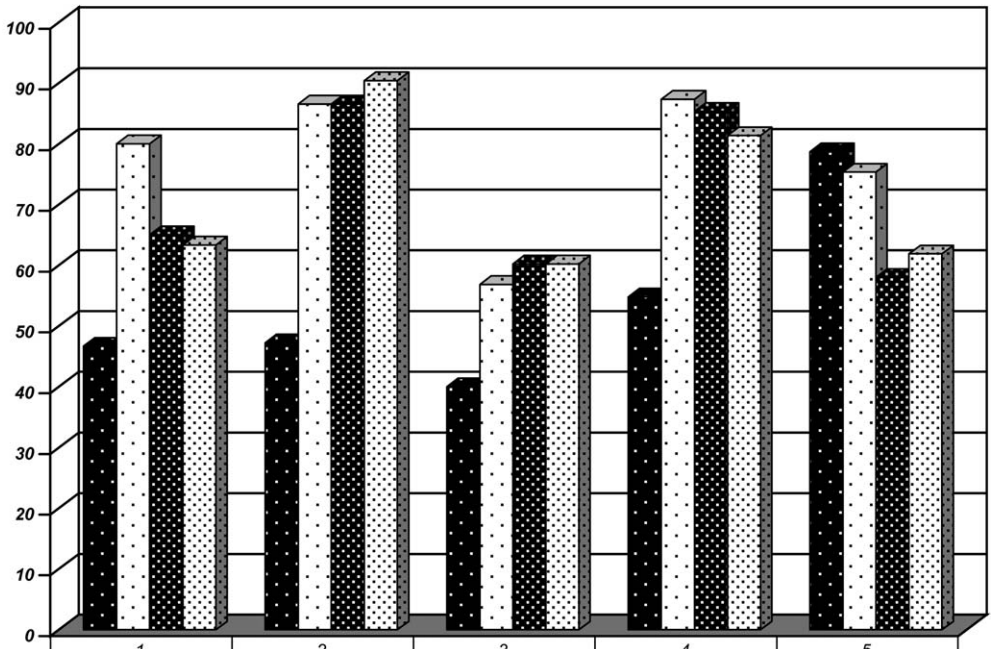

	1	2	3	4	5
GABOR	46.67	47.22	40	54.76	78.7
HAAR	80	86.54	56.82	87.33	75.34
DB2	65	86.54	60.23	85.33	57.99
DB4	63.33	90.385	60.227	81.33	61.9

Figure 19 PCBI score of Gabor, HAAR, DB2 and DB4 in normal images.

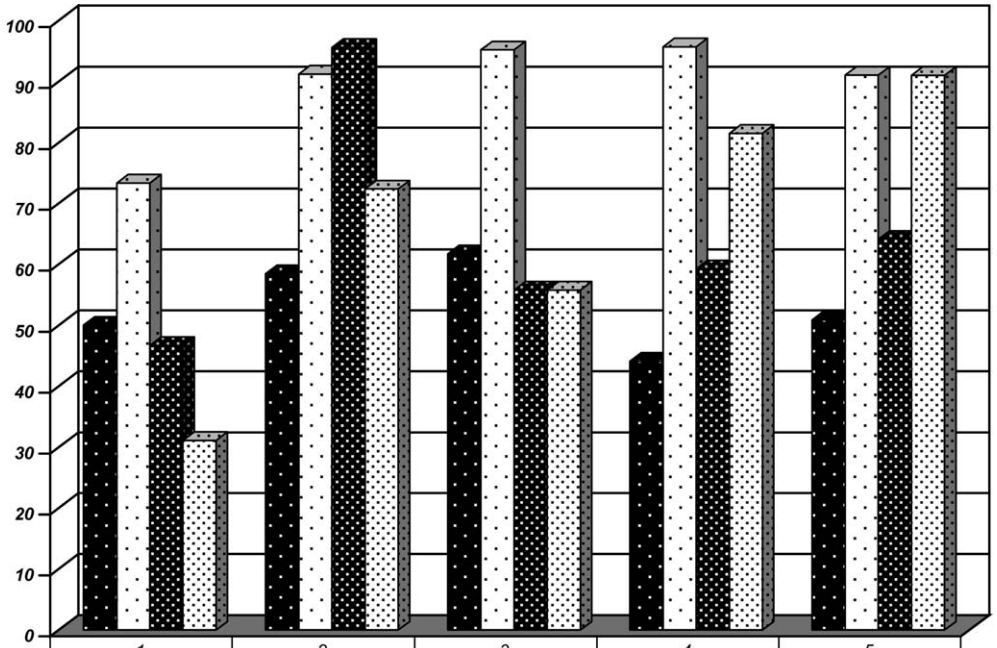

	1	2	3	4	5
GABOR	50	58.46	61.71	44.11	50.87
HAAR	73.33	91.25	95.19	95.73	91.03
DB2	46.67	95.62	55.77	59.26	64.1
DB4	31.11	72.39	55.77	81.48	91

Figure 20 PCBI score of Gabor, HAAR, DB2 and DB4 in less advanced stage of cancerous images.

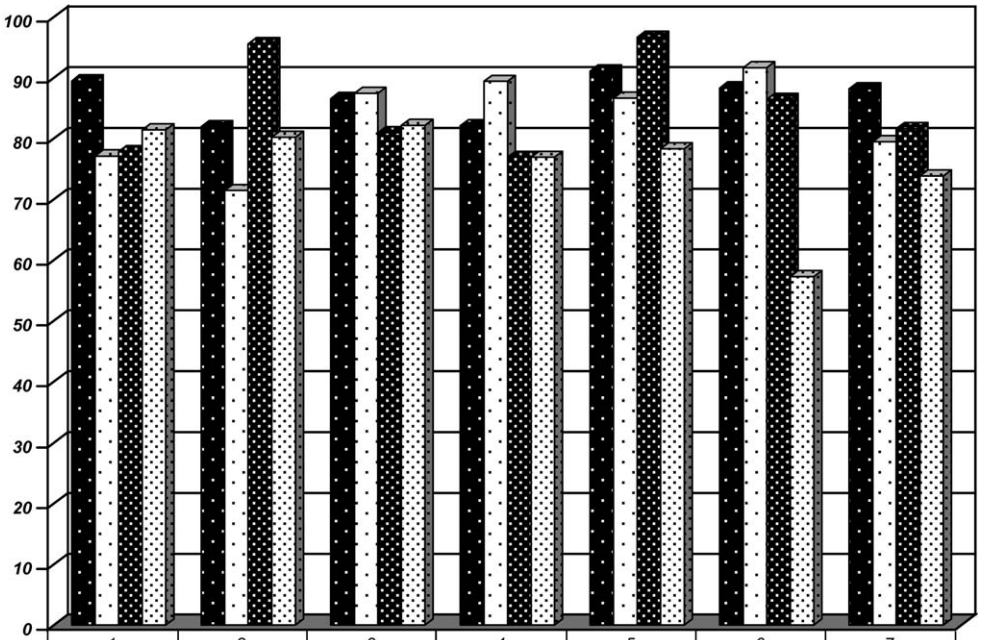

	1	2	3	4	5	6	7
GABOR	89.47	81.94	86.57	82.14	91.11	88.31	88.18
HAAR	77.14	71.43	87.45	89.42	86.67	91.67	79.5
DB2	77.86	95.61	80.98	76.92	96.67	86.46	81.65
DB4	81.43	80.22	82.19	76.92	78.33	57.29	73.86

Figure 21 PCBI score of Gabor, HAAR, DB2 and DB4 in advanced stage of cancerous images.

classifying normal, less advanced and more advanced stage of the disease than the other techniques. But interestingly, all the four techniques are equally effective in classifying the advanced stage of the disease. Thus these observations possibly have thrown some light in assessing the degree of difference between the normal and less advanced and advanced stage of the disease and higher sensitivity of HARR in distinguishing all three stages in respect to three other techniques possibly indicated that the tissue changes are more in between less advanced OSF and advanced OSF than the changes in between normal and less advanced state of the disease.

Conclusion

The present study proposes a novel ANN-based CAD detection technique for OSF. The TEM image of oral subepithelial collagen fibers (test image) has been subdivided into 64×64 contiguous pixel blocks. These blocks have undergone subband decomposition. The wavelet coefficients have been used by ANN for the selection of feature vector. Performance of four different wavelet functions, namely, GABOR, HAAR, DB2 and DB4 has been compared and it has been seen from the Table 6 that HAAR wavelet is performing to some extent better as an automatic diagnostic agent. It has been found that the HAAR wavelet is giving the above-specified performance with 1 hidden node less than that of DB2 and DB4 and 2 hidden nodes less than that of Gabor wavelet without a single misclassification. In case of less advanced stage of disease, some of the blocks are exhibiting the signature of normal collagen, whereas some are having the signature of advanced stage of OSF. If the final decision can be made considering the individual output of all four wavelet functions, the diagnosis will be far more accurate with better confidence. Fuzzy-MLP networks can be utilized to improve the diagnosis capability further in case of categorizing of finer grade of less-advanced stage of disease.

Acknowledgements

The microscopy part of the study was supported by the Research grant SP/SO/B-10/2001 from the Department of Science & Technology, Govt. of India. We thank Mr. S. N. Dey for excellent technical support in Electron Microscopy.

References

1. Parkin DM, Pisani P, Ferlay J. Estimates of the worldwide incidence of 25 major cancers in 1990. *Int J Cancer* 1999;**80**:827—41.
2. Wingo PA, Tong T, Bolden S. Cancer statistics, 1995. *CA Cancer J Clin* 1995;**45**:8—30.
3. Aziz SR. Oral submucous fibrosis: an unusual disease. *J N J Dent Assoc* 1997;**68**:17—9.
4. Canniff JP, Harvey W, Harris M. Oral submucous fibrosis: its pathogenesis and management. *Br Dent J* 1986;**160**:429—34.
5. Seedat HA, VanWyk CW. Betel-nut chewing and submucous fibrosis in Durban. *S Afr Med J* 1988;**74**:568—71.
6. Maher R, Lee AJ, Warnakulasuriya K, Lewis JA, Johnson NW. Role of areca nut in the causation of oral submucous fibrosis: acase-control study in Pakistan. *J Oral Pathol Med* 1994;**23**: 65—9.

7. Zain RB, Ikeda N, Razak IA, Axell T, Majid ZA, Gupta PC, et al. A national epidemiological survey of oral mucosal lesions in Malaysia. *Commun Dent Oral Epidemiol* 1997;**25**:377–83.
8. Canniff JP, Harvey W. The aetiology of oral submucous fibrosis: the stimulation of collagen synthesis by extracts of areca nut. *Int J Oral Surg* 1981;**10**(Suppl. 1):163–7.
9. Paul RR, Chatterjee J, Das AK, Cervera ML, de la Guardia M, Chaudhuri K. Altered elemental profile as indicator of homeostatic imbalance in pathogenesis of oral submucous fibrosis. *Biol Trace Elem Res* 2002;**87**:45–56.
10. Paul RR, Chatterjee J, Das AK, Dutta SK, Roy D. Zinc and iron as bioindicators of precancerous nature of oral submucous fibrosis. *Biol Trace Elem Res* 1996;**54**:213–30.
11. Pindborg JJ, Sirsat SM. Oral submucous fibrosis. *Oral Surg Oral Med Oral Pathol* 1966;**22**:764–79.
12. Nair UJ, Obe G, Friesen M, Goldberg MT, Bartsch H. Role of lime in the generation of reactive oxygen species from betel-quid ingredients. *Environ Health Perspect* 1992;**98**:203–5.
13. Van Wyk CW, Seedat HA, Philips VM. Collagen in submucous fibrosis: an electron microscopic study. *J Oral Pathol Med* 1990;**19**:182–7.
14. Paul RR, Mukherjee A, Dutta PK, Banerjee S, Pal M, Chatterjee J, et al. Pathological stage detection for oral precancerous condition using a novel wavelet-neural network-based technique. *J Clin Pathol* 2005;**58**:932–8.
15. Dayhoff JE, Deleo JM. Artificial neural network–opening the black box. *Cancer* 2001;**91**:1615–35.
16. Kappen HJ, Neijt JP. Advanced ovarian cancer. Neural network analysis to predict treatment outcome. *Ann Oncol* 1993;**4**(Suppl. 4): 31–4.
17. Maclin P, Dempsey J. Using an artificial neural network to diagnose hepatic masses. *J Med Syst* 1992;**16**:215–25.
18. Ravdin PM, Clark GM. A practical application of neural network analysis for predicting outcome of individual breast cancer patients. *Breast Cancer Res Treat* 1992;**22**:285–93.
19. Wilding P, Morgan MA, Grygotis AE, Shoffner MA, Rosato EF. Application of back propagation neural networks to diagnosis of breast and overian cancer. *Cancer Lett* 1994;**74**:143–53.
20. Wu Y, Giger ML, Doi K, Vyborny CJ, Schmidt RA, Metz CE. Artificial neural networks in mammography: application to decision making in the diagnosis of breast cancer. *Radiology* 1993;**187**:81–7.
21. Mishra A, Dutta PK, Ghosh MK. Non-rigid cardiac motion quantification from 2-D image sequences based on wavelet synthesis. *Image Vision Comput* 2001;**19**:929–39.
22. Chatterjee J, De K, Basu SK, Das AK. Collagen, zinc and iron contents of rat skin irradiated with chronic low-dose X-ray. *Indian J Med Res* 1993;**98**:243–7.
23. Faugeras O. *Three dimensional computer vision: a geometric viewpoint*. Massachusetts London, England: The MIT Press Cambridge; 1996.
24. Gabor D. Theory of communication. *J IEE (London)* 1946;**93**: 429–57.
25. Daugman J. Uncertainty relation for resolution in space, spatial frequency and orientation optimized by visual cortex filters. *J Opt Soc AM A* 1985;**2**:1160–9.
26. Manjunath B, Chellappa R. A computational approach to boundary detection. *IEEE conf CVPR*.
27. Super BJ, Bovik AC. Three dimensional orientation from texture using wavelets. In: *Proc. SPIE Conference of Visual Communications and Image Processings*, vol. 1606, 1991. p. 574–86.
28. Manjunath BS, Ma WY. Texture features for browsing and retrieval of image data. *IEEE Trans Pattern Anal Machine Intell* 1996;**18**:837–42.
29. http://www.mathworks.com/access/helpdesk/help/toolbox/wavelet/wavelet.html.
30. Daubechies I. *Ten lectures on wavelets*. Philadelphia, PA: SIAM; 1992.
31. Vellerli M, Herley C. Wavelet and filter banks: theory and design. *IEEE Trans Signal Process* 1992;**40**:2207–32.
32. Horn RA, Johnson CA. *Matrix analysis*. New York: Cambridge University Press; 1985.
33. Cybenko G. Approximation by superpositions of sigmoidal functions. *Math Control Signals Syst* 1989;**2**:303–14.
34. Demuth H, Beale M. *Neural network toolbox-for use with MATLAB-users guide*. MA, USA: The Mathworks Inc; 1993.
35. Duda OR, Hart PE, Stork DG. *Pattern classification*. Singapore: John Wiley & Sons; 2000.